

EFT triangles in the same-sign WW scattering process at the HL-LHC and HE-LHC

Geetanjali Chaudhary,^a Jan Kalinowski,^b Manjit Kaur,^a Paweł Kozów,^{bc} Kaur Sandeep,^a Michał Szleper^d and Sławomir Tkaczyk^e

^a *Panjab University, Chandigarh-160014, India*

^b *Faculty of Physics, University of Warsaw, ul. Pasteura 5, 02-093 Warsaw, Poland*

^c *CAFPE and Departamento de Física Teórica y del Cosmos, Universidad de Granada, Campus de Fuentenueva, 18071 Granada, Spain*

^d *National Center for Nuclear Research, High Energy Physics Department, ul. Pasteura 7, 02-093 Warsaw, Poland*

^e *Fermi National Accelerator Laboratory, Batavia, IL 60510, USA*

Abstract

We investigate the Beyond Standard Model discovery potential in the framework of the Effective Field Theory (EFT) for the same-sign WW scattering process in purely leptonic W decay modes at the High-Luminosity and High-Energy phases of the Large Hadron Collider (LHC). The commonly applied procedure of studying the $WWWW$ quartic coupling by testing dimension-8 operators of the EFT one at a time is used in this work. In the considered process there is no experimental handle on the WW invariant mass, and it has previously been shown that the discovery potential at 14 TeV is rather slim. In this paper we report the results calculated for a 27 TeV machine and compare them with the discovery potential obtained at 14 TeV. We find that while the respective discovery regions shift to lower values of the Wilson coefficients, the overall discovery potential of this procedure does not get significantly larger with a higher beam energy.

1 Introduction

The Large Hadron Collider (LHC) has completed data taking for Run II. While a lot of collected data still awaits to be analyzed, no physics Beyond the Standard Model (BSM) has been announced until now. The lack of direct indications for the presence of new physics (NP) makes indirect searches more interesting. The High Luminosity LHC (HL-LHC) upgrade will eventually collect an integrated luminosity of 3 ab^{-1} of data in pp collisions at a center-of-mass (c.o.m.) energy of 14 TeV, which should maximize the LHC potential to uncover new phenomena. It may however well be that the NP degrees of freedom are at higher masses making it difficult at the LHC to identify experimentally

new particles, or new paradigms. These considerations have been driving, in the last few years, intense activity worldwide to assess the future of collider experiments beyond the HL-LHC. Several proposals and studies have been performed. The prospects of pushing the LHC program further with the LHC tunnel and the whole CERN infrastructure, together with future magnet technology, is an exciting possibility that could push the energy up into an unexplored region with the 27 TeV High Energy LHC (HE-LHC), that could collect an integrated luminosity of 15 ab^{-1} .

Precision measurements provide an important tool to search for heavy BSM dynamics, associated with mass scales beyond the LHC direct energy reach, exploiting the fact that such dynamics can still have an impact on processes at smaller energy, via virtual effects. In this context the well-established framework of effective field theories (EFTs) allows to systematically parameterize BSM effects and elucidate how they modify SM processes. The BSM contributions are effectively parametrized in terms of higher dimension operators $\mathcal{O}_i^{(n)}$, with some effective couplings $C_i^{(n)}$ suppressed by appropriate powers of an unknown energy scale Λ at which new physics sets in,

$$\mathcal{L} = \mathcal{L}_{SM} + \sum_i \frac{C_i^{(6)}}{\Lambda^2} \mathcal{O}_i^{(6)} + \sum_i \frac{C_i^{(8)}}{\Lambda^4} \mathcal{O}_i^{(8)} + \dots, \quad (1.1)$$

where the superscript $n = 6, 8$ indicates the dimensionality of the corresponding operator. Following the usual notation, we introduce a set of Wilson coefficients $f_i^{(n)}$, defined as

$$f_i^{(6)} = \frac{C_i^{(6)}}{\Lambda^2}, \quad f_i^{(8)} = \frac{C_i^{(8)}}{\Lambda^4}, \dots, \quad (1.2)$$

which are free parameters since neither $C_i^{(n)}$ nor Λ of the full theory are known. Eq. (1.1) represents in principle an infinite and model-independent expansion, valid by construction up to the cutoff value Λ in the energy scale of the studied process. For practical reasons, however, data analysis is destined to be restricted to a limited number of chosen operators; it is therefore implicitly assumed that other operators will not play a role for the given process in the studied energy range. In particular, vector boson scattering (VBS) processes are widely recognized as the best laboratory to study dimension-8 operators, which modify only the $VVVV$ quartic couplings. In addition to skipping the dimension-6 ($n = 6$) operators, the usual procedure in VBS data analyses to date involves testing one dimension-8 operator at a time. Such a procedure breaks model independence of the EFT approach and raises a natural question of its physics usefulness.

In a recent paper [1] the physics potential of the single-operator EFT approach has been tested on a hypothetical new physics signal observed in the same-sign WW scattering process at the HL-LHC. The analysis was focused on the “gold-plated” purely leptonic W decay modes:

$$pp \rightarrow 2\text{jets} + l^+ \nu + l'^+ \bar{\nu}' \quad (1.3)$$

where l and l' stand for any combination of electrons and muons. In this process the M_{WW} invariant mass cannot be reconstructed experimentally on the event-by-event basis, leading to a restricted space in the (f_i, Λ) plane (the “EFT triangle”) for which the single-operator EFT description of the data is viable. In this note we extend such investigations to the HE-LHC energy and expected luminosity domain.

The paper is organized as follows. In Sec. 2 we remind the concept of “EFT triangles”. In Sec. 3, we detail our procedure of event simulation and subsequent treatment of generated events. In Sec. 4

we summarize our findings and conclude. Two Appendices contain supplementary material. In the first appendix we argue that qualitative features of the full WW scattering process, including off-shell effects, can be inferred from considering the on-shell WW scattering amplitudes and we discuss helicity amplitudes after adding the higher dimension operators. In the second appendix we address the question of what values of BSM couplings can be drawn from the discovery regions.

2 EFT triangles

Since the truncation of the expansion in Eq. (1.1) introduces model dependence, in Ref. [1] the concept of “EFT models” has been introduced where they are defined by the choice of operators $\mathcal{O}_i^{(n)}$ and the values of Wilson coefficients $f_i^{(n)}$. The EFT description is valid up to a cutoff energy Λ at which new states are expected to appear; the cutoff value is unknown a priori. However, in the presence of higher dimension operators the scattering amplitudes grow with energy and eventually break the perturbative unitarity limit M^U . The condition $\Lambda < M^U(f_i)$ defines the upper bound on the range of possible values of Λ as a function of f_i .

A specific feature of the process in Eq.(1.3) is that the scale $M \equiv M_{WW}$, i.e., the invariant mass of the scattered WW bosons, is not experimentally accessible, making it impossible to properly apply the cutoff Λ on the data. Any BSM signal, S , is defined as the deviation from the SM prediction in the differential distributions $d\sigma/dx_i$ of some observable x_i .

$$\frac{dS}{dx_i} = \left(\frac{d\sigma}{dx_i} \right)^{BSM} - \left(\frac{d\sigma}{dx_i} \right)^{SM}, \quad (2.1)$$

Any collected data sample will in general be a sum of the contributions from $M < \Lambda$ and $M > \Lambda$ (unless Λ happens to be out of kinematic reach). To cope with events with $M > \Lambda$, different solutions have been advocated in the literature, e.g.: from discarding these events at the level of simulation, to invoking unitarization procedures (usually assuming $\Lambda = M^U$) [2], [3], to ignoring the cutoff altogether. Any of the above prescriptions is related to additional arbitrariness of choices and therefore affects the physics interpretation of the results. Genuine data interpretation in the EFT language requires its successful description without any additional assumptions as to the nature of BSM physics at the scale above Λ . This is only possible if the bulk of the total observed BSM signal originates indeed from the EFT-controlled range.

The EFT-controlled signal reads:

$$\left(\frac{d\sigma}{dx_i} \right)^{EFT} = \int_{2M_W}^{\Lambda} \left(\frac{d^2\sigma}{dx_i dM} \right)^{EFT} dM + \int_{\Lambda}^{M_{max}} \left(\frac{d^2\sigma}{dx_i dM} \right)^{SM} dM, \quad (2.2)$$

Here M_{max} is the kinematic limit of the WW invariant mass. Eq. (2.2) defines signal coming uniquely from the “EFT model” in its range of validity and assumes only the SM contribution in the region $M > \Lambda$.

The additional contribution from the region above Λ may enhance the signal, but it may also preclude proper description of the data within the EFT. The total BSM signal can be estimated without detailed knowledge of the UV completion from the expected asymptotic behavior for $M \rightarrow \infty$, i.e., by assuming that all the helicity amplitudes above Λ remain constant at their respective

values they reach at Λ (hence superscript $A = \text{const}$):

$$\left(\frac{d\sigma}{dx_i}\right)^{\text{BSM}} = \int_{2M_W}^{\Lambda} \left(\frac{d^2\sigma}{dx_i dM}\right)^{\text{EFT}} dM + \int_{\Lambda}^{M_{\text{max}}} \left(\frac{d^2\sigma}{dx_i dM}\right)^{A=\text{const}} dM, \quad (2.3)$$

For every value of Λ , BSM observability imposes some minimum value of f_i for which the total BSM signal defined by Eq.(2.3) has enough statistical significance, 5σ in our example. Successful description in the EFT framework imposes some maximum value of f_i such that signal estimates computed from Eqs.(2.2) and (2.3) remain statistically consistent, e.g., within 2σ . The “EFT triangle” is the region in the (f_i, Λ) plane for which a statistically significant BSM signal can be successfully described with a chosen higher dimension operator \mathcal{O}_i . It is bounded from three sides:

- from above by the unitarity limit $M^U(f_i)$,
- from the left by the signal significance of 5σ , computed according to Eq. (2.3),
- and from the right by the consistency within 2σ with Eq. (2.2).

In the HL-LHC case, for all the individual dimension-8 operators that affect the $WWWW$ quartic coupling such triangles were found to be rather narrow or even entirely empty (for \mathcal{O}_{S1}) [1]. In this paper we extend this analysis to the HE-LHC case, in an attempt to verify if an increased beam energy and integrated luminosity will translate into larger EFT triangles.

Throughout this work we follow the MadGraph convention for the definition of dimension-8 operators (implemented therein via public UFO files), in which the field strength tensors $W_{\mu\nu} \equiv \frac{i}{2}g\tau^i(\partial_\mu W_\nu^i - \partial_\nu W_\mu^i + g\epsilon_{ijk}W_\mu^j W_\nu^k)$ are replaced with $\hat{W}_{\mu\nu} \equiv \frac{1}{ig}W_{\mu\nu}$. Such conversion factors are equivalent to absorbing the electroweak coupling constants g , each one explicitly factored out for each occurrence of the field stress tensor, in the effective couplings C_i . For details, see Ref. [4].

3 Analysis

In this section we present a generator-level study aimed at finding the EFT triangles for the individual $n = 8$ operators at the HE-LHC. Event samples of the process $pp \rightarrow jj\mu^+\mu^+\nu\nu$ at 27 TeV were generated for each $n = 8$ operator \mathcal{O}_i that modifies the $WWWW$ quartic coupling, $i = S0, S1$ (so called scalar operators), $T0, T1, T2$ (transverse), and $M0, M1, M6, M7$ (mixed¹ ones). Generation has been done at LO using MadGraph5_aMC@NLO v5.2.6.2 generator [5], with the appropriate UFO files containing additional vertices involving the desired $n = 8$ operators. A scan of f_i values for each operator was made using the MadGraph `reweight` command, including $f_i = 0$ to represent the SM case. The Pythia package v6.4.1.9 [6] was used for hadronization as well as initial and final state radiation processes. Unitarity limits were determined using the VBFNLO [7] calculator v1.4.0, after applying appropriate Wilson coefficients conversion factors. Cross sections at the output of MadGraph were multiplied by a factor 4 to account for all the lepton (electron and/or muon) combinations in the final state (in this work only positively charged leptons are taken into account, although the same analysis can be done for the negative charges). Only signal samples were generated and the SM case was treated as irreducible background in the study of possible BSM

¹ $M6$ is redundant: $\mathcal{O}_{M6} = \frac{1}{2}\mathcal{O}_{M0}$; we omit this operator in further analysis.

effects. Reducible background for this process is known to be strongly detector dependent and was not considered in this analysis.

The applied analysis chain to the events generated for HE-LHC is a carbon copy of the one described in detail in Ref. [1]. All event selection criteria are kept the same, namely we require at least two reconstructed jets and exactly two leptons (muons or electrons) satisfying the following conditions: $M_{jj} > 500$ GeV, $\Delta\eta_{jj} > 2.5$, $p_T^j > 30$ GeV, $|\eta_j| < 5$, $p_T^l > 25$ GeV and $|\eta_l| < 2.5$. We disregard the fact that an increased beam energy may lead to a re-optimization of the detector geometries and of selection criteria in order to accommodate for the slightly different event topologies. Like before, the total BSM signal is estimated according to Eq.(2.3) by suppressing the high-mass tail above the calculated value of Λ . This is achieved by applying an additional weight of the form $(\Lambda/M_{WW})^4$ to each generated event in this region. The EFT-controlled signal is calculated according to Eq.(2.2) by replacing the generated high-mass tail with the one expected in the SM (known as “clipping method”). Signal significances are computed as the square root of a χ^2 resulting from a bin-by-bin comparison of the event yields, with statistical errors such as expected from the data at 3 ab^{-1} , in the distribution of the most sensitive kinematic variables. Compared to the 14 TeV analysis, the binning of histograms was changed so that in the highest bin the SM prediction normalized to $3/\text{ab}$ is still between 2-3 events. In Fig. 1 as an example shown are distributions of four chosen variables:

- invariant mass of two leptons M_{ll} ,
- ratio of transverse momenta of leptons and jets $R_{p_T} \equiv p_T^{l1}p_T^{l2}/(p_T^{j1}p_T^{j2})$,
- $M_{o1} \equiv \sqrt{(|\vec{p}_T^{l1}| + |\vec{p}_T^{l2}| + |\vec{p}_T^{miss}|)^2 - (\vec{p}_T^{l1} + \vec{p}_T^{l2} + \vec{p}_T^{miss})^2}$
- and the (true) invariant mass M_{WW}

in the SM and in the case $f_{M1} = 0.2 \text{ TeV}^{-4}$ and $\Lambda = 4.9 \text{ TeV}$. As it was for 14 TeV, we found R_{p_T} to be the most sensitive kinematic variable for \mathcal{O}_{S0} and \mathcal{O}_{S1} , and M_{o1} for the remaining operators.

As the unitarity limit we take always the lower of the two values between on-shell W^+W^+ and on-shell W^+W^- scattering, calculated from T-matrix diagonalization in the helicity space. Indeed, both processes probe the same quartic coupling and are governed by the same Wilson coefficients, as further explained in Appendix A.3.

Fig. 2 shows the results for the individual operators $S0, S1, T0, T1, T2, M0, M1$ and $M7$, in comparison with results at 14 TeV (for positive f values). Not unexpectedly, all the triangles are shifted to lower f values compared to 14 TeV, the shift being as large as almost an order of magnitude. However, the total area of the triangles does not get significantly larger as we increase the energy. This is because the EFT consistency criterion pushes the effective upper limits on f in a similar manner as does the BSM observability criterion for the lower limits. Overall, the shapes and sizes of all the EFT triangles are remarkably similar for 27 TeV as for 14 TeV, only their respective positions differ.

Fig. 3 shows the respective results for negative f values of $S0, S1, T0, T1, T2, M1$ and $M7$. Here exactly the same observations can be made again. The negative f values of $M0$ look virtually identical to their positive counterparts, since for these operators the SM-BSM interference term in the total amplitude calculation is practically negligible (see the Appendix for details), and so we do not show them here. There is no triangle at all for $S1$, for which the overall lower limit for BSM

observability is about 1.2 TeV^{-4} and the upper limit for EFT consistency is 1.4 TeV^{-4} . Here as well we observe a similar behavior as for 14 TeV. Such as for 14 TeV, full detector simulation with reducible backgrounds included can only make the picture worse.

For the sake of a convenient comparison between the respective results at two different pp beam energies, in the bulk of this study we have always assumed the same integrated luminosity of 3 ab^{-1} for both cases. This number is appropriate for the HL-LHC stage, but underestimates the expected statistical power of the HE-LHC. However, it is trivial to recalculate all the results to $15/\text{ab}$ in order to get the true expected discovery reach of the HE-LHC, taking into account its actual expected luminosity. An increase of statistics by a factor 5 will lead to a further shift of all the EFT triangles by a factor close to $\sqrt{5}$, both in the 5σ discovery and the 2σ consistency curves (in fact, somewhat less than that because of non-linear dependence of the BSM signal on the value of the individual Wilson coefficients). It will not significantly change either the shape nor the size of triangles. A comparison of results calculated for the same pp beam energy of 27 TeV and two different integrated luminosities is exemplified for the $M1$ operator in Fig. 4.

Our simple procedure to suppress the high-mass tails by applying a $(\Lambda/M_{WW})^4$ weight to events generated above the scale of Λ works reasonably well in the vicinity of the unitarity limit. In this region it produces a tail falling approximately like $1/M_{WW}^2$, which is the expected asymptotic (i.e., for $M_{WW} \gg \Lambda$) behavior of the total cross section after regularization. It nonetheless becomes too strong as we go to $\Lambda \ll M^U$, where the total cross section is still dominated by the SM contribution which does not require any further suppression. Moreover, for low values of Λ the tail itself becomes large, leading to large uncertainties due to the details of its modeling. We have discontinued the curves on Figs. 2 and 3 below the values at which we find the method lead to the unphysical result of signal being suppressed below the SM level itself. For this reason the EFT triangles for $T0, T1$ and $T2$ do not close. For the remaining cases, however, they are completely contained in the region where our simple method is still viable.

4 Conclusion and Outlook

Although an increase of the LHC energy vastly improves the sensitivity to new physics effects in VBS processes, the question of EFT applicability is a different one and cannot be solved by changing the energy. The same-sign WW process with its purely leptonic W decays is often considered “gold-plated” due to its relatively good signal to background ratio, but the lack of experimental access to the WW invariant mass poses a severe problem in describing the data in terms of the EFT. Despite reasonable sensitivity to BSM effects, such effects if observed will most likely not be possible to interpret using the data from this process alone and applying the usual framework of testing one dimension-8 operator at a time. This conclusion holds regardless of the actual proton beam energy.

The present results reinforce the former conclusion that future VBS data analysis, both at the LHC experiments as well as future proton-proton colliders, should evolve in the direction of multidimensional fits with many higher dimension operators varied at a time. This in turn may require global simultaneous fits to many processes (including WZ , ZZ and semi-leptonic WW , if not other processes) to help disentangle the correlations between signals originating from different operators.

Helpful in disentangling the effects of different operators may be also the polarizations of the

outgoing W bosons, as different operator subsets, S, T and M, affect different polarizations. There are new theoretical ideas how to project the total VBS cross sections onto individual polarizations without invoking the rather crude W on-shell approximation [8]. WW polarizations can be extracted from the data by fitting simulated templates of the corresponding polarized distributions. Unfortunately, purely leptonic WW decays do not offer the possibility to reconstruct the W decay angle, which is the only strictly model-independent signature of W polarization. While many other distributions exhibit qualitative differences between the different polarizations, they are usually also strongly model-dependent. Consequently, SM templates cannot be used in the BSM case without the risk of losing sensitivity to the BSM signal. If, however, a set of observables is identified for which sufficiently model-independent templates for $W_L W_L$, $W_T W_T$ and $W_T W_L$ can be constructed, it could vastly improve the perspectives of future VBS data analysis in the framework of the EFT.

Acknowledgments

We would like to thank Adam Falkowski and Luca Merlo for valuable comments and discussions. The work of PK is supported by the Spanish MINECO project FPA2016-78220-C3-1- P (Fondos FEDER) and by National Science Centre, Poland, the PRELUDIUM project under contract 2018/29/N/ST2/01153. JK was supported in part by the National Science Centre, Poland, the HARMONIA project under contract UMO-2015/18/M/ST2/00518 (2016-2020). JK and MS were partly supported by the COST Action CA15108 and are grateful to all the members of the Action for inspiring discussions. ST is supported by Fermi Research Alliance, LLC under Contract No. De-AC02-07CH11359 with the United States Department of Energy.

A WW scattering: off-shell versus on-shell

In this Appendix we investigate what can be said about the VBS subprocess in the full $pp \rightarrow jjll'\nu_l\nu_{l'}$ reaction from the analysis of the on-shell WW scattering process. We start with the discussion of the WW scattering in full pp process, then identify the helicity amplitudes that dominate the high-energy behavior in the presence of dimension-8 operators and discuss the question of determining the unitarity limits.

A.1 WW scattering in the full pp reaction

In the physical process $pp \rightarrow jjll'\nu_l\nu_{l'}$ the W bosons are off-shell. Nevertheless, in this subsection we would like to show that qualitative conclusions on the influence of dimension-8 operators on the full process can be drawn from the analysis of on-shell WW scattering. To this end, let us employ the identity [8]:

$$g_{\mu\nu} + \frac{k_\mu k_\nu}{M_W^2} = \sum_{\lambda=1}^4 \epsilon_\lambda^\mu(k) (\epsilon_\lambda^\nu(k))^*. \quad (\text{A.1})$$

to express the numerator of the off-shell vector boson as a sum over polarization vectors $\epsilon_\lambda^\mu(k)$. In the frame in which the spatial component of k_μ is in the z direction, $k_\mu = (E, 0, 0, k)$, the explicit

form of each polarization vector reads:

$$\begin{aligned}\epsilon_-^\mu &= \frac{1}{\sqrt{2}}(0, +1 - i, 0) && \text{(left),} \\ \epsilon_+^\mu &= \frac{1}{\sqrt{2}}(0, -1 - i, 0) && \text{(right),} \\ \epsilon_0^\mu &= (k, 0, 0, E)/\sqrt{k^2} && \text{(longitudinal),} \\ \epsilon_A^\mu &= (E, 0, 0, k)/\sqrt{\frac{k^2 - M_W^2}{k^2 M_W^2}} && \text{(auxiliary),}\end{aligned}\quad (\text{A.2})$$

where $k^2 \equiv k_\mu k^\mu$. In the on-shell limit $k^2 \rightarrow M_W^2$ the auxiliary polarization vanishes and ϵ_0 approaches the exact on-shell form of longitudinal polarization. With the help of eq. (A.1) one can then rewrite each of the 4 W propagators in each of the diagram that has VBS topology, as

$$\frac{-i \sum_{\lambda=1}^4 \epsilon_\lambda^\mu (\epsilon_\lambda^\nu)^*}{k^2 - M_W^2}. \quad (\text{A.3})$$

Then the parton-level amplitude $qq \rightarrow qql'l'v_lv'_l$ with VBS topology can be decomposed as follows

$$M \equiv \frac{\sum_{\lambda_1 \lambda_2 \lambda_3 \lambda_4} M_{\lambda_1}^{q1} M_{\lambda_2}^{q2} M_{\lambda_1 \lambda_2 \lambda_3 \lambda_4}^{WW} M_{\lambda_3}^{l1} M_{\lambda_4}^{l2}}{(k_1^2 - M_W^2)(k_2^2 - M_W^2)(k_3^2 - M_W^2)(k_4^2 - M_W^2)}, \quad \lambda_i \in \{\epsilon_-, \epsilon_+, \epsilon_0, \epsilon_A\}. \quad (\text{A.4})$$

The $M_{\lambda_i}^{qi}$ ($M_{\lambda_i}^{li}$) terms are the trilinear qqW (llW) vertices contracted with ϵ^* (ϵ) of eq. (A.3), while the $M_{\lambda_1 \lambda_2 \lambda_3 \lambda_4}^{WW}$ term is the (off-shell) WW elastic scattering amplitude. The sum over i includes necessarily polarization configurations in which the W polarizations are auxiliary. Now, the effect of dimension-8 operators grows with the scattering energy $M_{WW} \gg M_W$ and modifies significantly helicity amplitudes so that deviations from the SM behavior become non-negligible. Since the off-shellness k_i^2 are suppressed dynamically by propagators $1/(k_i^2 - M_W^2)$, in this kinematic limit the scattered vector bosons must be fast, $|\vec{k}_i| \sim E_i \gg M_W$. Therefore in the high M_{WW} region $\epsilon_0^\mu \sim \epsilon_A^\mu$ and approach the on-shell form of the longitudinal polarization vector. As a result, the sum in eq. (A.3) runs effectively over $\epsilon_i = \epsilon_0, \epsilon_+, \epsilon_-$ and the off-shell helicity amplitude can be approximated by the on-shell one, accounting corrections of order $\sqrt{(k^2 - M_W^2)/(k^2 M_W^2)}$ or $1/\sqrt{k^2}$. Therefore in the following subsections we will discuss in detail the high-energy behavior of on-shell WW scattering in the presence of contributions from dimension-8 operators and the unitarity bound.

A.2 The on-shell WW scattering and the helicity amplitudes

Let us consider the elastic on-shell $W^+W^+ \rightarrow W^+W^+$ in the presence of BSM part represented by a single dimension-8 operator, as in an "EFT model". The scattering amplitude iM can be written as:

$$iM = A_{SM} + A_{BSM}, \quad (\text{A.5})$$

where A_{SM} denotes the SM part and A_{BSM} represents the BSM part that depends on the Wilson coefficients f_i .

For the on-shell W bosons we choose to work in the helicity basis in which the polarizations are ϵ_i^μ with $i = +, -, 0..$. There are in total $3^4 = 81$ helicity amplitudes $iM(ij \rightarrow kl)$ corresponding to helicity configurations $(ijkl)$ in the $WW \rightarrow WW$ scattering process. The total unpolarized on-shell WW cross section can schematically be written as:

$$\sigma \sim \frac{1}{9} \sum_{i,j,k,l} |A_{SM}(ij \rightarrow kl)|^2 + (A_{SM}(ij \rightarrow kl) A_{BSM}(ij \rightarrow kl)^* + h.c.) + |A_{BSM}(ij \rightarrow kl)|^2 \quad (\text{A.6})$$

Since there are orders of magnitude differences concerning contributions of different helicity amplitudes to the total cross section it is convenient, using discrete symmetries \mathcal{P} and \mathcal{T} and Bose statistics, to divide 81 polarization amplitudes into classes. Amplitudes from the same class yield the same contribution to (polarized) cross sections. Hence, in practice one can consider a reduced number of 13 independent polarization classes, taking into account their multiplicities when computing the cross section. It turns out that only a few helicity configurations contribute non-negligibly at high WW scattering energy. We refer to such helicities as saturating helicities.

For the case of the SM the contribution from the saturating helicities to the total unpolarized cross-section is shown in Fig. 5. The four saturating helicity configurations are the only ones whose scattering amplitude is asymptotically constant in energy. The remaining helicity configurations behave asymptotically at most as $1/s$, hence their contribution is strongly suppression at large $s = M_{WW}^2$.

In the presence of $n = 8$ operators some of the saturating helicities grow with s , maximally as s^2 . The corresponding case for each “EFT model” studied is shown in figs. 6 and 7 for $f_i > 0$ and $f_i < 0$, respectively. In fact, for each “EFT model” there is at least one polarization configuration with the asymptotic s^2 energy dependence providing dominant contribution to the unpolarized cross section at $M_{WW} = M^U$. In particular, in the case of “EFT models” with scalar operators (S) only the amplitude with all W bosons polarized longitudinally grows as s^2 . In the case of transverse operators (T) some amplitudes with all W polarized transversally grow as s^2 , while for the case of mixed operators (M) it happens for amplitudes with two longitudinal and two transverse polarizations. It follows from $D_\mu \Phi$ and $W_{\mu\nu}$ building blocks of BSM operators which project mostly on the longitudinal and transverse modes, respectively. It is interesting to notice, however, that for different S , T and M distinct polarization configurations of the outgoing W ’s dominate the total cross section at large M_{WW} . Measurement of final state W polarizations would give an insight to the dynamics of their interactions.

Since helicity is an observable for the on-shell WW scattering reaction, different helicity configurations do not interfere among themselves. The total unpolarized elastic on-shell WW cross sections as a function of the center of mass WW energy and its dependence on the f_i sign is shown in Fig. 8. The sign dependence of the total unpolarized cross section, most visible for $T0$, $T2$ and also present for $T1$, $M1$, $M7$, $S0$, $S1$, is due to the interference terms in eq. (A.6). More precisely, the dependence on the sign of the f_i is determined by the magnitude of SM-BSM terms relative to the BSM² ones in the region $E \lesssim \Lambda \leq M^U$. While there are always BSM² terms that asymptotically behave as s^4/Λ^8 , the earlier growth as $\sim s^2/\Lambda^4$ of the interference terms is not necessarily visible in each of the “EFT models”. If the helicity configurations for which the amplitude depends on energy as s^2 are not among the saturating helicities of the SM, extra suppression factor(s) of $v/\Lambda \ll 1$ with respect to the opposite case, will be present in the SM-BSM terms. The latter means suppressed sign dependence of the unpolarized cross section, i.e. suppressed interference. It can be inferred from the polarization decomposition plots in figs. 6, 7 that it is the case for the $M0$ operator, and indeed in Fig. 8 it is seen that the interference effect is practically invisible for this operator.

Although for the off-shell bosons the helicities are not observable and amplitudes with different helicity configurations may interfere, their interference will be dumped by different structures of fermionic currents to which they are coupled.

$i =$	$S0$	$S1$	$T0$	$T1$	$T2$	$M0$	$M1$	$M7$
$f_i > 0$	0000	0000	— — — and — — + +	— — + +	— — — —	— — 00	— — 00	— — 00
$f_i < 0$	0000	0000	— — + +	— — + +	— — + +	— — 00	— — 00	— — 00

Table 1: The helicity combinations yielding the strongest helicity partial waves unitarity limits for each operator in case of each sign of f_i . It is always a $J=0$ partial wave that yields the strongest unitarity limits

A.3 The unitarity bound

The dominating polarization configurations in the total unpolarized cross section can be read from figs. 6, 7. However, the helicity combination that determines the M^U , i.e. that yields strongest unitarity bound, is not necessarily among them. The reason is as follows. The partial wave expansion of helicity amplitude starts with $J_{\min} = \max\{|\lambda_1 - \lambda_2|, |\lambda_3 - \lambda_4|\}$, where $\lambda_{1,2}$ and $\lambda_{3,4}$ correspond initial and final W polarizations, and it is the $J = J_{\min}$ partial wave that yields the strongest unitarity limit. It has been checked that for the same-sign WW helicity amplitude that depends on energy as s^2 for the case of M operators $J_{\min} = 1$, while for the S and T operators $J_{\min} = 0$. It would imply then that the unitarity limit for the M operators would be weaker than for S and T , especially if only the $J = 0$ partial waves were considered. However, the same operators affect both the same-sign and opposite-sign WW scattering processes, and both processes should be considered for the determination of the unitarity bounds. In the case of the latter reaction the number of independent helicity configurations is 17 resulting from the fact that one can use all three \mathcal{C} , \mathcal{P} and \mathcal{T} symmetries; however one cannot use the Bose symmetry. In this case for each “EFT model”, including the M ones, there exists a helicity configuration that depends on energy as s^2 and has $J_{\min} = 0$. As a result, for the M -type “EFT model” the unitarity limit is considerably stronger as compared to the limit derived from same-sign WW partial wave expansion. This should be kept in mind in particular when using a VBFNLO calculator to determine the unitarity bounds that both same- and opposite-sign WW scattering processes are looked at. The helicity combination yielding the strongest helicity partial wave unitarity limits for each operator are summed up in Table 1.

B Extracting the BSM coupling from the discovery regions found

Assuming that the departure from the SM predictions is indeed observed at the HL/HE-LHC we turn to the question what can be said about the couplings of higher dimension operators that defined the “EFT model”. While the probed Λ scale can be read off directly from figs. 2, 3, the matching between fundamental parameters C_i of a deeper BSM physics and the Wilson coefficients f_i of the low energy approximation is needed to extract the information about couplings.

Let us start with operators that contain the stress tensor $W_{\mu\nu}$. The W bosons, being fundamental $SU(2)$ gauge bosons, would couple to the to-be-integrated-out BSM states via gauge coupling g . Therefore from the corresponding f_i one can factor out g^2 for each $W_{\mu\nu}$. The Naive Dimensional Analysis (NDA) [9] suggests then the following matching

$$\begin{aligned}
\mathcal{L} \supset f_i \mathcal{O}_i &\equiv c_i \cdot 2 \frac{g^2}{\Lambda^4} \mathcal{O}_i, \quad i = M0, M1 \\
f_i \mathcal{O}_i &\equiv c_i \cdot 2^2 \frac{g^4}{16\pi^2 \Lambda^4} \mathcal{O}_i, \quad i = T0, T1, T2 \\
f_i \mathcal{O}_i &\equiv c_i \cdot 2^2 \frac{g^2}{\Lambda^4} \mathcal{O}_i, \quad i = M6, M7
\end{aligned} \tag{B.1}$$

The factor 2 follows from the relation $\text{Tr} \hat{W}_{\alpha\beta} \hat{W}_{\mu\nu} = \frac{1}{2} W_{\alpha\beta}^i W_{\mu\nu}^i$ since in NDA the stress tensor $W_{\mu\nu}^i$ is used for counting purposes rather than the matrix form $\hat{W}_{\mu\nu}$. Extra factor 2 in case of $M6, M7$ operators is due to differences in the $SU(2)$ structure, as can be seen from the relation $\mathcal{O}_{M7} = \frac{1}{2} \mathcal{O}_{M1} + \dots$, while $\frac{1}{16\pi^2}$ in front of T operators is a single loop suppression factor suggested by the 4-th power of the electroweak coupling factored out.

The remaining dimensionless factors c_i could be combinations of

$$\frac{g_*}{4\pi}, \quad \frac{y_*}{4\pi}, \quad \frac{\lambda_*}{16\pi^2}, \tag{B.2}$$

where g_* , y_* and λ_* are some gauge, Yukawa and scalar couplings of the BSM sector of full theory, respectively. In the weakly-coupled theory one would expect that c_i are naturally of order 1.

Using (B.1) it is straightforward to find the range of c_i corresponding to the discovery regions shown in Fig. 2, 3. The numerical values, presented in Table 2 and 3 for 27 and 14 TeV case, respectively, are found to be roughly consistent. However, instead of being of order 1 they are much

$f_i > 0$	$T0$	$T1$	$T2$	$M0$	$M1$	$M7$
$c_{min} - c_{max}$	130.-770.	120.-1300.	670.-2200.	23.-32.	45.-133.	33.-140.

$f_i < 0$	$T0$	$T1$	$T2$	$M1$	$M7$
$c_{min} - c_{max}$	110.-1500.	140.-2600.	410.-4500.	48.-130.	54.-270.

Table 2: For each “EFT model” characterized by a choice of a single $n = 8$ operator shown are the ranges of the overall coefficients c_i in eq. B.1 that correspond to the discovery regions found in the 27 TeV study.

$f_i > 0$	$T0$	$T1$	$T2$	$M0$	$M1$	$M7$
$c_{min} - c_{max}$	137.-790.	76.-1300.	280.-2200.	23.-33.	38.-140.	24.-130.

$f_i < 0$	$T0$	$T1$	$T2$	$M0$	$M1$	$M7$
$c_{min} - c_{max}$	510.-1400.	170.-1200.	700.-4100.	23.-33.	45.-140.	24.-140.

Table 3: See Table 2 for description; 14 TeV case.

larger. It suggests that in case of linearly realized spontaneous breaking of $SU(2) \times U(1)$ symmetry

our method of probing BSM physics is sensitive only to strong dynamics. Alternatively one could consider relaxed assumptions concerning the symmetry breaking mechanism For the analysis on “EFT triangles” in the so-called Higgs Effective Field Theory [10], see [11].

We turn now to the discussion of the $S0$ and $S1$ operators. We assume these are generated at loop level in the BSM. Otherwise they would come associated with $n = 6$ operators, which are neglected in our analysis. Then, the NDA suggests

$$\mathcal{L} \supset f_i \mathcal{O}_i \equiv c_i \cdot \frac{g_*^4}{16\pi^2 \Lambda^4} \mathcal{O}_i, \quad i = S0, S1 \quad (\text{B.3})$$

Again, c_i are some combinations of BSM couplings and naturally expected to be of order 1. If we set $c_i = 1$ in eq. (B.3), then for $f_{S0} > 0$ we find that that $g_* \in (8.5; 10.)$ and $g_* \in (8.4; 10.)$ in the 14 and 27 TeV case respectively. For $f_{S0} < 0$ we find $g_* \in (6.2; 8.9)$ and $g_* \in (7.3; 8.8)$ for the 14 and 27 TeV case, respectively. The coupling is large, but interestingly it satisfies $g_* < 4\pi$. For f_{S1} the discovery regions are empty for both 14 and 27 TeV cases for both signs.

References

- [1] J. Kalinowski, P. Kozów, S. Pokorski, J. Rosiek, M. Szleper, S. Tkaczyk, Eur. Phys. J. C (2018) 78: 403, doi: 10.1140/epjc/s10052-018-5885-y [[arXiv:1802.02366](https://arxiv.org/abs/1802.02366) [hep-ph]].
- [2] A. Alboteanu, W. Kilian and J. Reuter, JHEP **0811**, 010 (2008) doi:10.1088/1126-6708/2008/11/010 [[arXiv:0806.4145](https://arxiv.org/abs/0806.4145) [hep-ph]].
- [3] W. Kilian, T. Ohl, J. Reuter and M. Sekulla, Phys. Rev. D **91**, 096007 (2015) doi:10.1103/PhysRevD.91.096007 [[arXiv:1408.6207](https://arxiv.org/abs/1408.6207) [hep-ph]].
- [4] C. Degrande *et al.*, [[arXiv:1309.7890](https://arxiv.org/abs/1309.7890) [hep-ph]].
- [5] J. Alwall *et al.*, JHEP **07** (2014) 079, doi:10.1007/JHEP07(2014)079 [[arXiv:1405.0301](https://arxiv.org/abs/1405.0301) [hep-ph]].
- [6] T. Sjostrand, S. Mrenna, P. Skands, JHEP **0605** (2016) 026, doi:10.1088/1126-6708/2006/05/026 [[arXiv:hep-ph/0603175](https://arxiv.org/abs/hep-ph/0603175)].
- [7] K. Arnold *et al.*, Comput. Phys. Commun. **180** (2009) 1661, doi:10.1016/j.cpc.2009.03.006 [[arXiv:0811.4559](https://arxiv.org/abs/0811.4559) [hep-ph]]; J. Baglio *et al.* [arXiv:1107.4038](https://arxiv.org/abs/1107.4038) [hep-ph], [arXiv:1404.3940](https://arxiv.org/abs/1404.3940) [hep-ph].
- [8] A. Ballestrero, E. Maina and G. Pelliccioli, J. High Energ. Phys. (2018) 2018: 170, doi: 10.1007/JHEP03(2018)170 [[arXiv:1710.09339](https://arxiv.org/abs/1710.09339) [hep-ph]].
- [9] B. M. Gavela, E. E. Jenkins, A. V. Manohar and L. Merlo, Eur. Phys. J. C **76** (2016) no.9, 485 doi:10.1140/epjc/s10052-016-4332-1 [[arXiv:1601.07551](https://arxiv.org/abs/1601.07551) [hep-ph]].
- [10] R. Alonso, M. B. Gavela, L. Merlo, S. Rigolin and J. Yepes, Phys. Lett. B **722**, 330 (2013) Erratum: [Phys. Lett. B **726**, 926 (2013)] doi:10.1016/j.physletb.2013.04.037, 10.1016/j.physletb.2013.09.028 [[arXiv:1212.3305](https://arxiv.org/abs/1212.3305) [hep-ph]].
- [11] P. Kozów, L. Merlo, S. Pokorski and M. Szleper, [[arXiv:1905.03354](https://arxiv.org/abs/1905.03354) [hep-ph]]

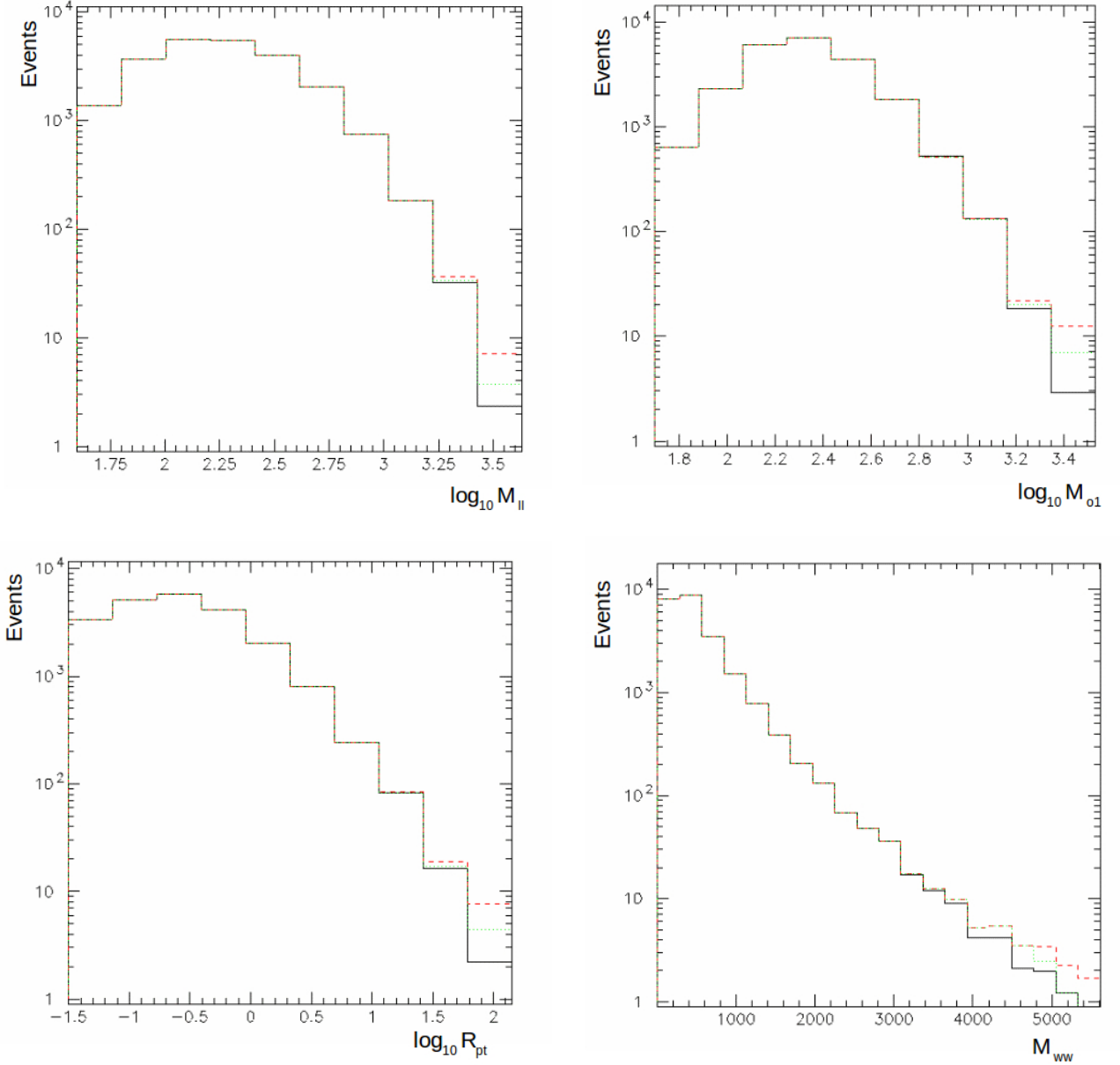


Figure 1: Typical examples of kinematic distributions used for the assessment of BSM signal significances. Shown are the distributions of M_{ll} , M_{o1} and R_{pT} (in log scale): in the Standard Model (black), with $f_{M1} = 0.2 \text{ TeV}^{-4}$ and the high- M_{WW} tail treatment according to Eq. (2.3) (red), and with $f_{M1} = 0.2 \text{ TeV}^{-4}$ and the high- M_{WW} tail treatment according to Eq. (2.2) (green). In addition the lower-right plot shows the distribution in the invariant mass of the WW system, M_{WW} with $f_{M1} = 0.2 \text{ TeV}^{-4}$. In all the plots the scale Λ was chosen as: $\Lambda = M^U = 4.9 \text{ TeV}$. Assumed is $\sqrt{s} = 27 \text{ TeV}$ and an integrated luminosity of 3 ab^{-1} .

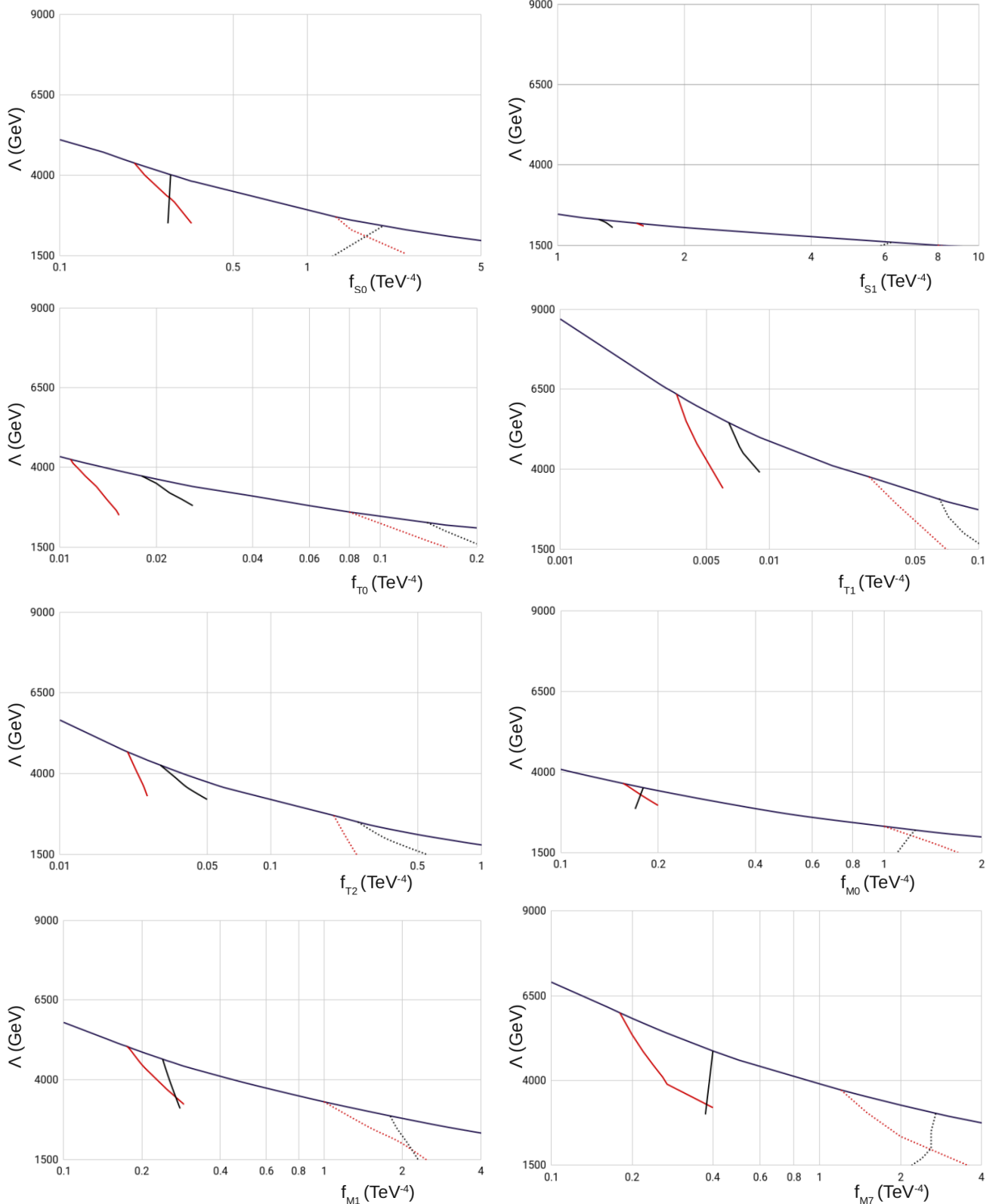


Figure 2: Regions in the Λ vs f (positive f values) space for dimension-8 operators in which a 5σ BSM signal can be observed and the EFT is applicable. The unitarity limit is shown in blue; the lower limits for a 5σ signal significance from Eq. (2.3) (red) and the upper limit on 2σ EFT consistency (black). The solid (dotted) lines correspond to $\sqrt{s} = 27$ (14) TeV. Assumed is the integrated luminosity of 3 ab^{-1} .

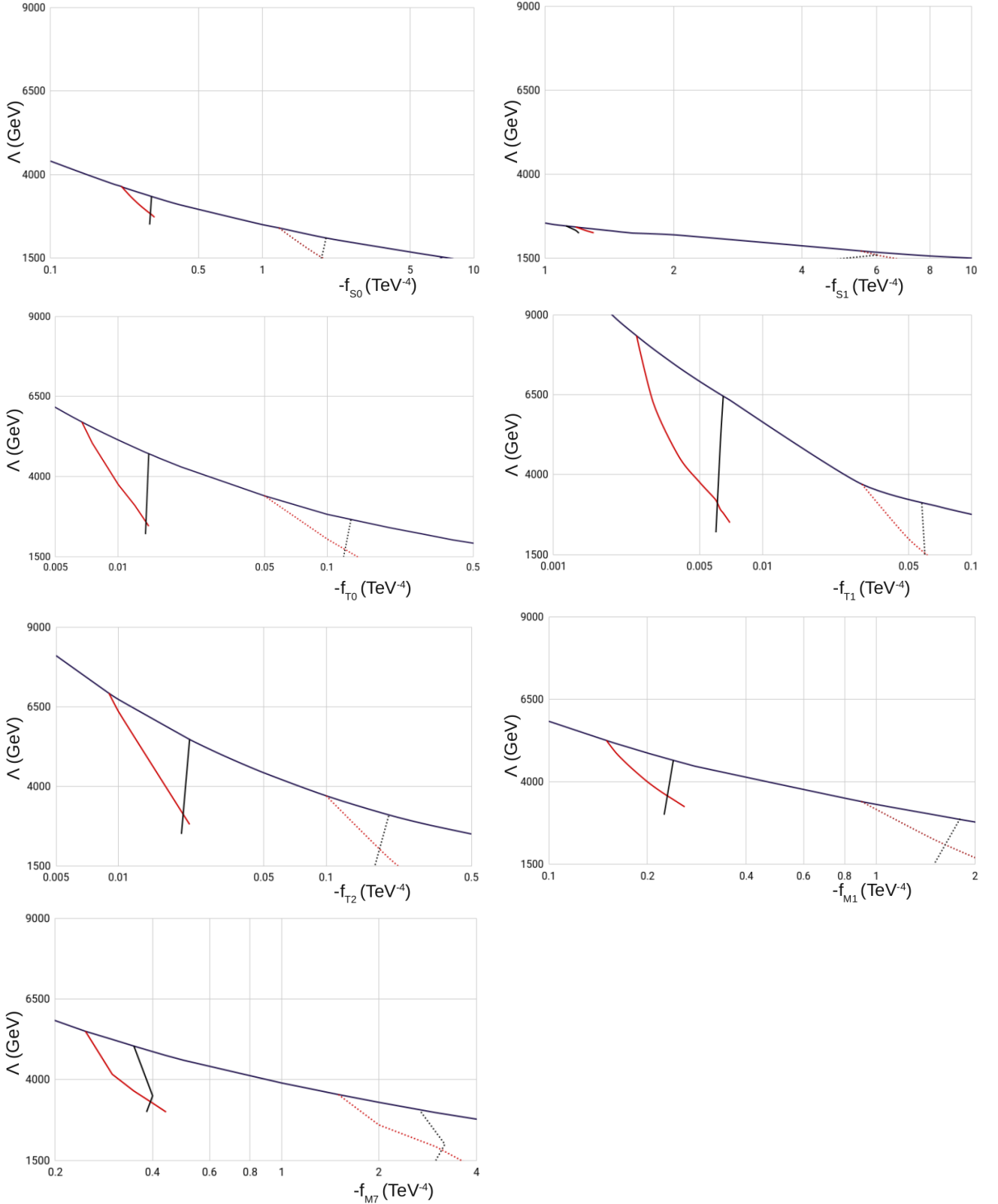


Figure 3: Regions in the Λ vs f (negative f values) space for dimension-8 operators in which a 5σ BSM signal can be observed and the EFT is applicable. The unitarity limit is shown in blue; the lower limits for a 5σ signal significance from Eq. (2.3) (red) and the upper limit on 2σ EFT consistency (black). The solid (dotted) lines correspond to $\sqrt{s} = 27$ (14) TeV. Assumed is the integrated luminosity of 3 ab^{-1} .

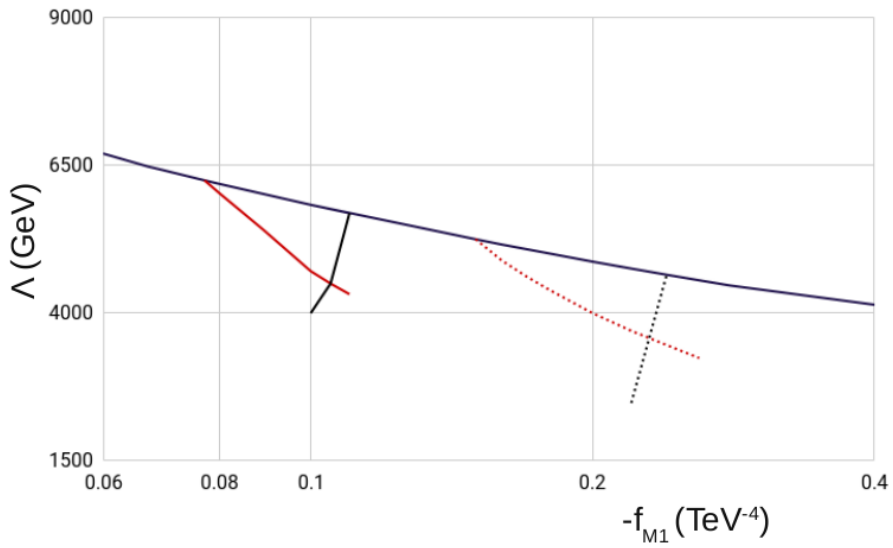


Figure 4: Regions in the Λ vs f (negative f values) space for $M1$ operator in which a 5σ BSM signal can be observed and the EFT is applicable. The unitarity limit is shown in blue; the lower limits for a 5σ signal significance from Eq. (2.3) (red) and the upper limit on 2σ EFT consistency (black). The solid (dotted) lines correspond to 15 ab^{-1} (3 ab^{-1}). Assumed is $\sqrt{s} = 27 \text{ TeV}$.

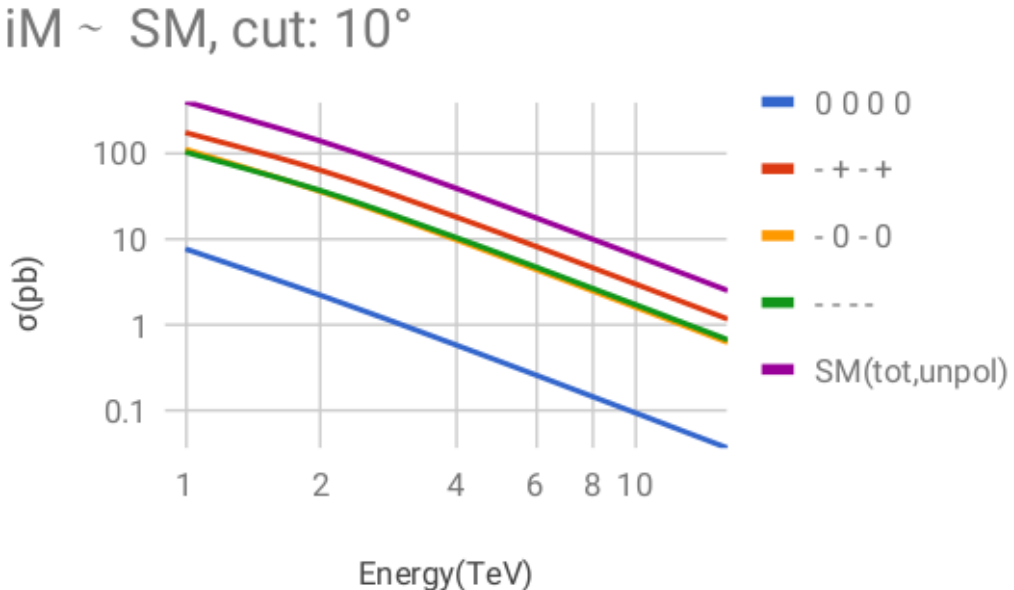


Figure 5: Contributions of various helicity configurations (multiplicity taken into account) to the total unpolarized cross section as a function of the center-of-mass collision energy ($E_{CM} \equiv \sqrt{s}$, in TeV) in the SM. The total unpolarized cross section is shown in violet.

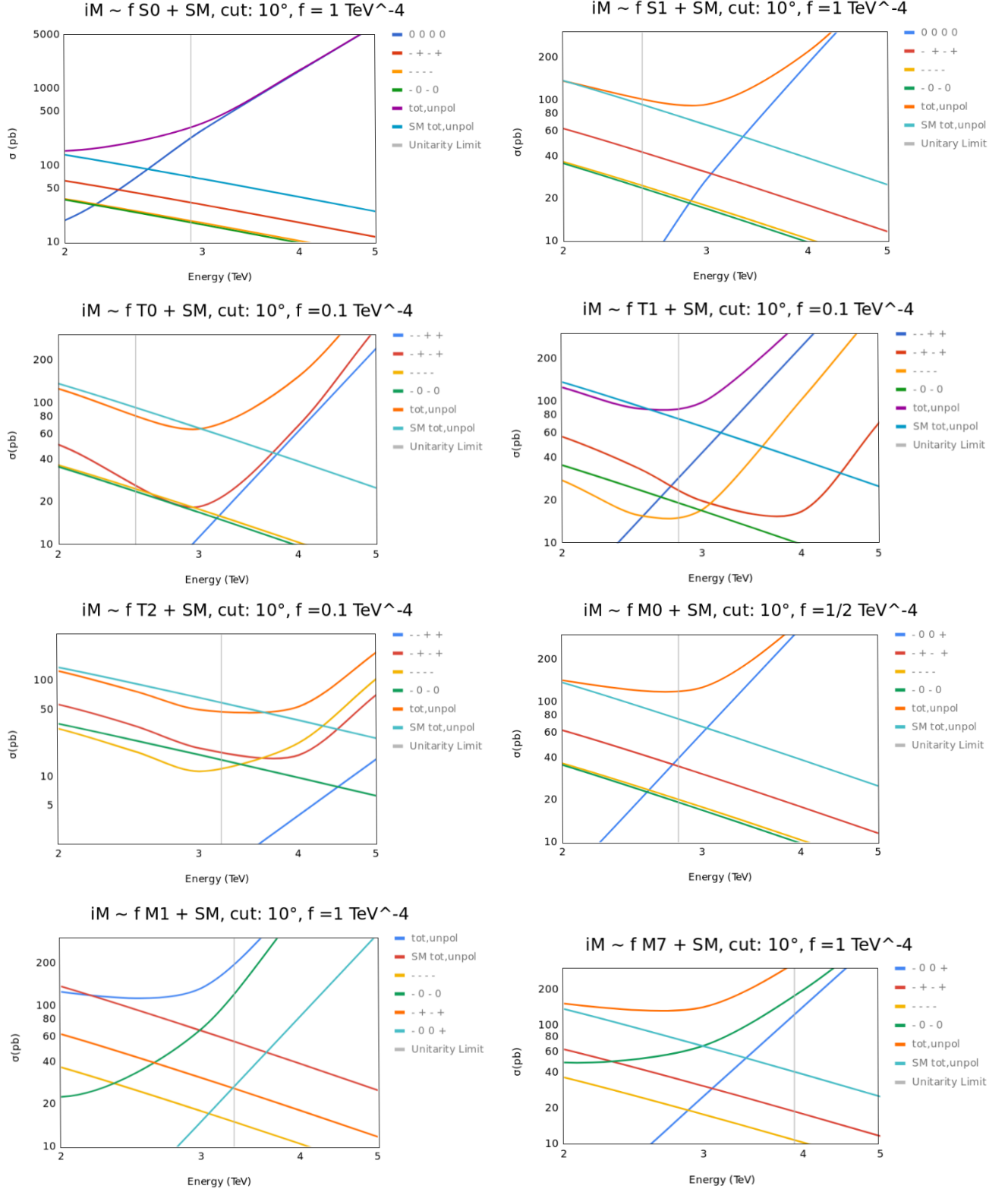


Figure 6: Contributions of the polarized cross sections (multiplicity taken into account) as functions of the center-of-mass collision energy ($E_{CM} \equiv \sqrt{s}$, in TeV) for chosen values of $f_i > 0$. The remaining (not shown) polarized cross sections are negligibly small. In each plot shown is in addition the total cross section of a EFT "model" and the total cross section in the SM.

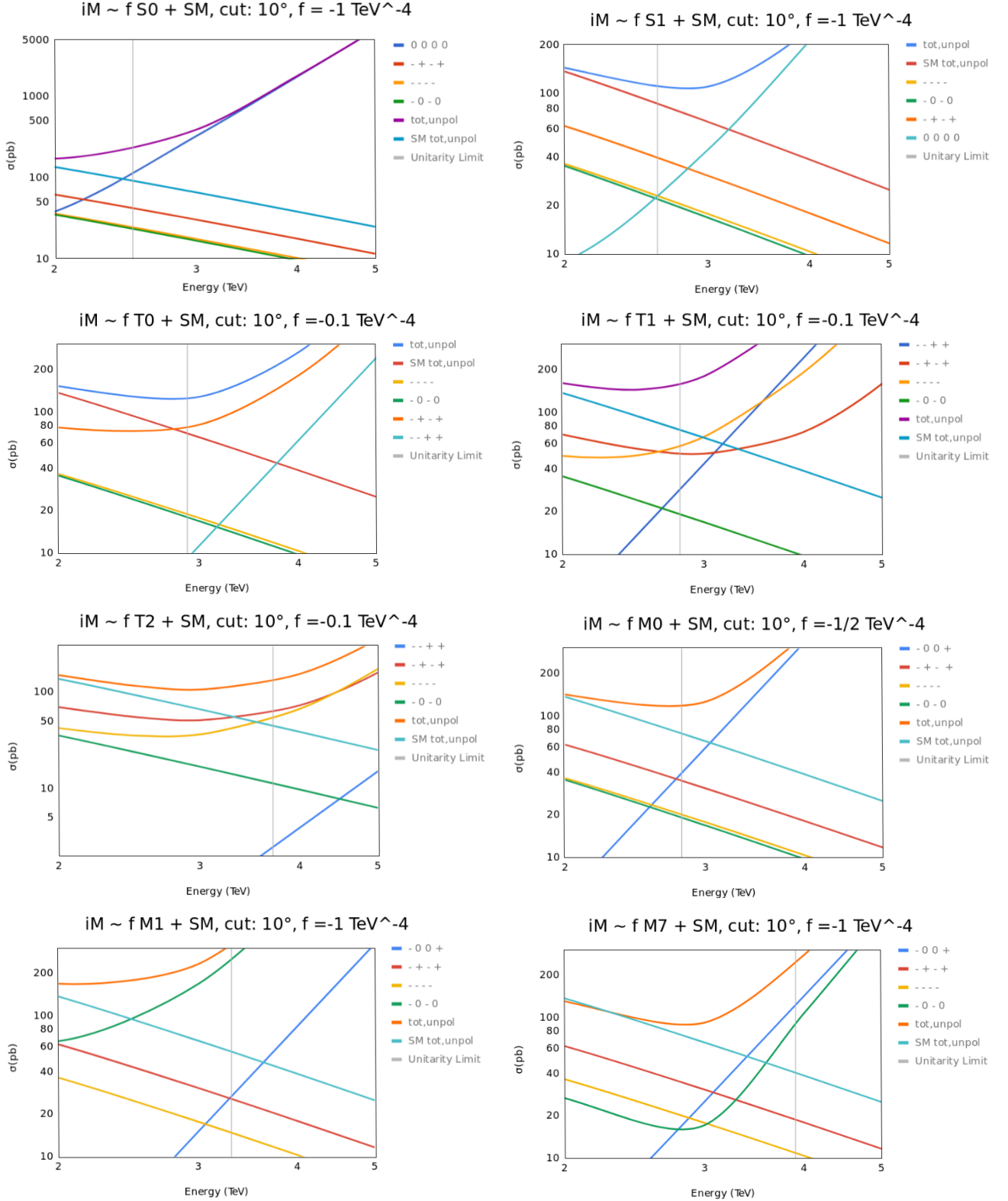


Figure 7: Contributions of the polarized cross sections (multiplicity taken into account) as functions of the center-of-mass collision energy ($E_{CM} \equiv \sqrt{s}$, in TeV) for chosen values of $f_i < 0$. The remaining (not shown) polarized cross sections are negligibly small. In each plot shown is in addition the total cross section of a EFT "model" and the total cross section in the SM.

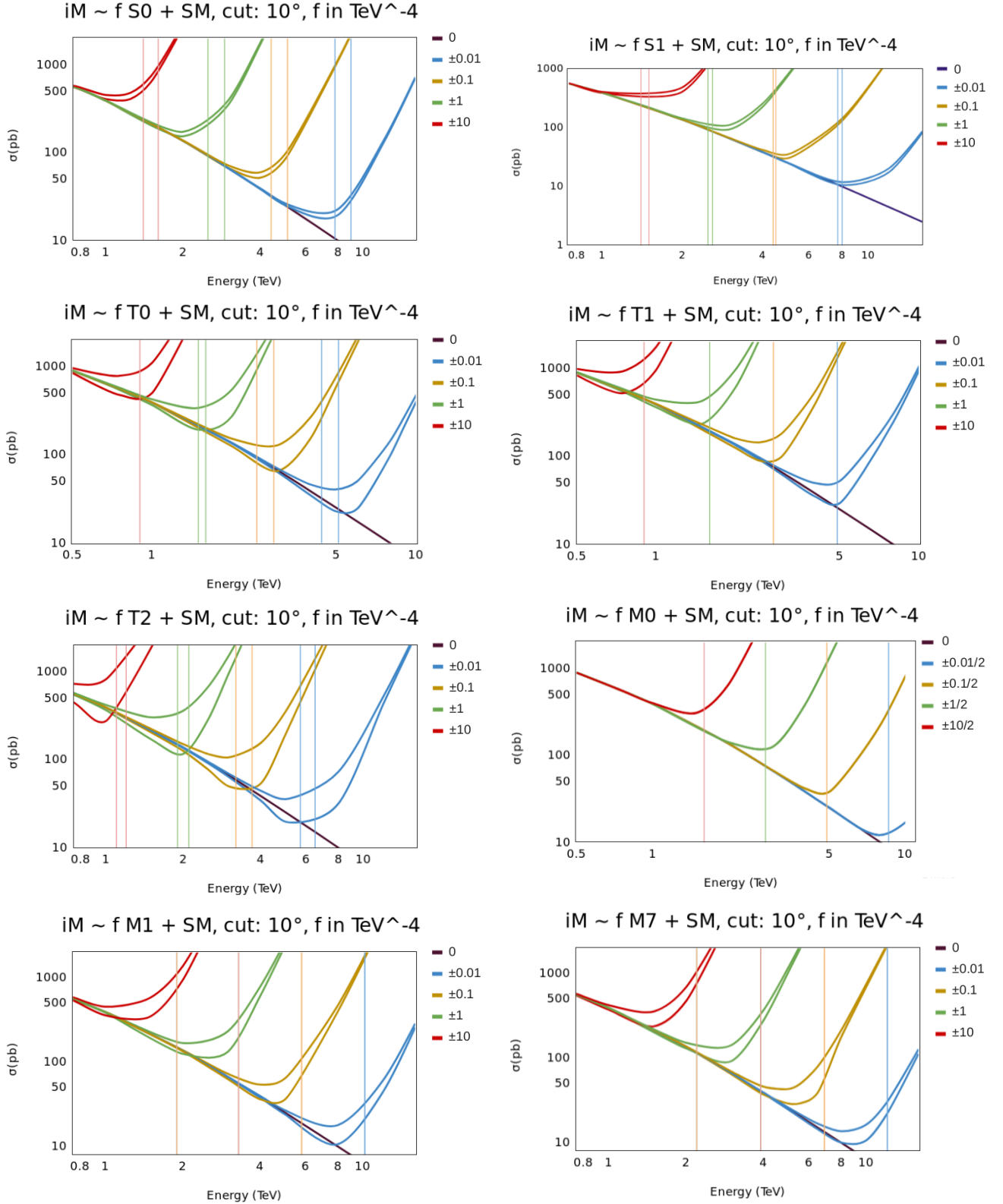


Figure 8: Energy dependence of the total unpolarized W^+W^+ cross sections ($E_{CM} \equiv \sqrt{s}$, in TeV) for a chosen set of f_i values. Vertical lines denote the unitarity bound $\sqrt{s^U}$ (color correspondence). There is no color distinction between the signs: except for $M1$ and $M7$, upper cross section curves correspond to $f < 0$; in $S0$, $S1$ ($T0$, $T2$) stronger unitarity limits correspond to $f < 0$ ($f > 0$).